

Crystal Structures of *Candida albicans* N-Myristoyltransferase with Two Distinct Inhibitors

Satoshi Sogabe,^{1,3} Miyako Masubuchi,¹
Kiyooki Sakata,¹ Takaaki A. Fukami,¹
Kenji Morikami,¹ Yasuhiko Shiratori,¹
Hirosato Ebiike,¹ Kenichi Kawasaki,¹
Yuko Aoki,¹ Nobuo Shimma,¹ Allan D'Arcy,^{2,4}
Fritz K. Winkler,^{2,5} David W. Banner,²
and Tatsuo Ohtsuka¹

¹Nippon Roche Research Center
200 Kajiwara
Kamakura, Kanagawa 247-8530
Japan

²Pharmaceutical Research
F. Hoffmann-La Roche Ltd.
CH-4070 Basel
Switzerland

Summary

Myristoyl-CoA:protein N-myristoyltransferase (Nmt) is a monomeric enzyme that catalyzes the transfer of the fatty acid myristate from myristoyl-CoA to the N-terminal glycine residue of a variety of eukaryotic and viral proteins. Genetic and biochemical studies have established that Nmt is an attractive target for antifungal drugs. We present here crystal structures of *C. albicans* Nmt complexed with two classes of inhibitor competitive for peptide substrates. One is a peptidic inhibitor designed from the peptide substrate; the other is a nonpeptidic inhibitor having a benzofuran core. Both inhibitors are bound into the same binding groove, generated by some structural rearrangements of the enzyme, with the peptidic inhibitor showing a substrate-like binding mode and the nonpeptidic inhibitor binding differently. Further, site-directed mutagenesis for *C. albicans* Nmt has been utilized in order to define explicitly which amino acids are critical for inhibitor binding. The results suggest that the enzyme has some degree of flexibility for substrate binding and provide valuable information for inhibitor design.

Introduction

Myristoyl-CoA:protein N-myristoyltransferase (Nmt; EC 2.3.1.97) catalyzes the transfer of the 14-carbon saturated fatty acid myristate (tetradecanoate; C14:0) from myristoyl-CoA to the N-terminal glycine residue of a variety of eukaryotic cellular and viral proteins [1–3]. This covalent modification via an amide linkage occurs cotranslationally in eukaryotes after the first methionine is removed by a methionyl-aminopeptidase [4, 5]. The covalent attachment of myristate results in an increase of lipophilicity that triggers association with cellular

membranes and that facilitates interactions with hydrophobic protein domains [6, 7]. Nmt participates in diverse biological processes, including signal transduction cascades [8] and apoptosis [9].

Nmt from *Saccharomyces cerevisiae* has been cloned and well characterized in its enzymatic function, substrate and acyl-CoA binding specificity [10]. Substrate binding and kinetic studies with myristoyl-CoA and its analogs have indicated that catalysis by Nmt occurs via an ordered Bi-Bi mechanism [11]. The apo-enzyme first forms a myristoyl-CoA:Nmt binary complex with high selectivity for myristoyl-CoA. A peptide substrate then binds to generate a myristoyl-CoA:Nmt:peptide ternary complex. Following the catalytic transfer of myristate from CoA to peptide substrate, free CoA is released first and the N-myristoylated peptide second.

Several Nmts have been cloned from the important pathogenic fungi *Candida albicans* [12], *Cryptococcus neoformans* [13], and *Aspergillus fumigatus* (K. Hashido, personal communication). Genetic experiments have established that the *NMT* gene is essential for vegetative growth and survival of *C. albicans* [14] and *C. neoformans* [15]. Human Nmt has also been cloned and characterized [16]. *C. albicans* Nmt has 451 amino-acid residues, with a sequence identity of 45% to the human enzyme. Clear differences in the peptide-substrate specificity between fungal and human Nmts have been exploited, and Nmt has been identified as a potential chemotherapeutic target for antifungal agents [17–19].

A peptidomimetic inhibitor, SC-58272, showing selectivity between the *C. albicans* and human enzymes has been designed and synthesized by elaboration of peptide substrates (Table 1) [20]. SC-58272 is competitive for the binding of peptide substrates, contingent upon prior binding of myristoyl-CoA as for a peptidic inhibitor, ALYASKLS-NH₂ [17], derived from the N-terminal fragment of *S. cerevisiae* Arf2p. Recently, we identified selective nonpeptidic inhibitors by in vitro enzyme inhibitory assay screening and then optimized them using a medicinal chemistry approach (Table 1) [21, 22]. Complete details of our efforts to develop the nonpeptidic compounds will be published elsewhere. These inhibitors are competitive for the binding of peptide substrates as well as SC-58272 and are highly selective for *C. albicans* Nmt over the human Nmt. Some of them showed in vivo antifungal activity in an animal model. Other types of nonpeptidic inhibitors have been reported, although their in vivo efficacy has not been described [23–25].

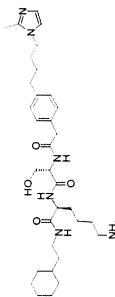
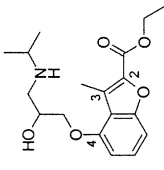
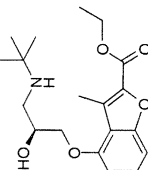
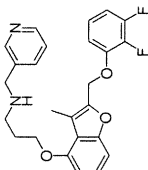
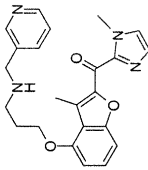
X-ray crystal structures of Nmt from two different species have been determined. The *C. albicans* apo-enzyme structure has been refined to 2.45 Å resolution (Protein Data Bank ID code 1NMT) [26]. The structure of *S. cerevisiae* Nmt with a nonhydrolyzable myristoyl-CoA analog [S-(2-oxo)pentadecyl-CoA] and a dipeptide inhibitor (SC-58272) has been refined to 2.9 Å resolution (Protein Data Bank ID code 2NMT) [27]. Recently, the binary complex of *S. cerevisiae* Nmt with myristoyl-CoA and the ternary complex of *S. cerevisiae* Nmt with S-(2-oxo)

³Correspondence: satoshi.sogabe@roche.com

⁴Present address: Morphochem AG, Schwarzwaldallee 215, WRO-1055, CH-4058 Basel, Switzerland.

⁵Present address: Life Sciences, Paul Scherrer Institut, CH-5232 Villigen PSI, Switzerland.

Table 1. Chemical Structures and Enzyme Inhibition of Peptidic and Non peptidic Inhibitors of Nmt

	1	2	3	4	5
					
Structure					
Enzyme inhibition* (μM)					
CaNmt	0.83	1.1	0.03	0.004	0.001
HsNmt	>140	>570	88	62	69

* Inhibitory activity against *C. albicans* Nmt (CaNmt) and human Nmt (HsNmt) as assessed by IC₅₀ using myristoyl-CoA (0.5 μM) and peptide substrate GLTISKLFRR-NH₂ (0.5 μM) and GNAASARR-NH₂ (0.5 μM), respectively.

pentadecyl-CoA and an octapeptide substrate (GLY-ASKLA) have been determined at 2.2 Å and 2.5 Å resolution, respectively (Protein Data Bank ID codes 1IIC and 1IID) [28]. The structure of the *C. albicans* apo-enzyme revealed a unique α/β fold [26]. The ternary complexes of *S. cerevisiae* Nmt have addressed substrate specificity and the catalytic mechanism [27, 29]. The three-dimensional structure of *C. albicans* Nmt with nonpeptidic inhibitors would also contribute to the rational design of potent compounds to selectively inhibit the fungal enzyme while remaining nontoxic to mammalian cells. We present here the determination of the crystal structures of the complex of *C. albicans* Nmt with two different classes of inhibitor. One is the peptidomimetic inhibitor (SC-58272 [30]), and the other is nonpeptidic (Table 1). We also describe an extensive mutagenesis study to elucidate the inhibitor contact regions. These results provide not only valuable information for structure-based drug design but also some insights into the structural features of the catalytic reaction of Nmt.

Results and Discussion

Overall Structure

The ternary complex of *C. albicans* Nmt with myristoyl-CoA and SC-58272, a peptidic inhibitor, was determined at 2.3 Å resolution. The model contains 392 residues (residues 60 to 451), myristoyl-CoA, SC-58272, and 123 solvent molecules, and has good stereochemistry (Table 2). The average root-mean-square deviation (rmsd) of C α atoms between the two molecules in the asymmetric unit is 0.6 Å. Crystal structures of *C. albicans* Nmt with nonpeptidic inhibitors were also determined at 3.2 (or 3.5) Å resolution by soaking experiments. Crystals of the apo-enzyme had relatively higher solvent contents than those of the ternary complex, which may explain the susceptibility of these crystals to X-ray damage. The model is comprised of residues 71 to 107 and 114 to 451 of each Nmt monomer. The average rmsd of C α atoms among the four molecules (molecules A to D) in the asymmetric unit was 0.4 Å, the structure being refined with tight noncrystallographic symmetric restraints between the polypeptide chains for residues 82 to 451. The inhibitors were bound to two of the four molecules (A and C) in the asymmetric unit, whereas the other two molecules (B and D) had relatively higher B factors with poor electron density. Average B factors for molecules A and C were 38.4 Å² and 38.2 Å², respectively, whereas those of molecules B and D were 48.7 Å² and 56.4 Å², respectively. Molecule C is the focus of the structural discussion in this work. As evidenced by its poor electron density, the loop of residues 108 to 113 (defined as the Ab loop [28], see below) was disordered in *C. albicans* Nmt complexed with nonpeptidic inhibitors as well as the *C. albicans* apo-enzyme crystallized with different crystallographic symmetry [26].

The protein fold of *C. albicans* Nmt in complexes with inhibitors consists of a compact saddle-shaped β sheet flanked on both of its faces by several α helices. The overall structure is the same as those of the *S. cerevisiae* Nmt complex [27] and the *C. albicans* apo-enzyme [26], with typical rmsds of C α atoms of 1.9 Å and 1.2 Å,

Table 2. Refinement Statistics

Enzyme Cofactor Compound	CaNmt Myristoyl-CoA SC-58272	CaNmt – 2	CaNmt – 4	CaNmt – 5
Crystal properties				
Space group	P2 ₁ 2 ₁ 2 ₁	P2 ₁ 2 ₁ 2 ₁	P2 ₁ 2 ₁ 2 ₁	P2 ₁ 2 ₁ 2 ₁
Unit cell (Å)	58.7, 95.3, 176.5	93.3, 94.9, 267.9	93.6, 96.7, 270.1	93.3, 96.9, 269.3
Data collection				
Resolution (Å)	2.3	3.5	3.2	3.2
Completeness (%)	92.2	93.7	81.0	99.0
R _{sym} ^a (%)	0.065	0.118	0.098	0.072
Refinement ^b				
Resolution range (Å)	40–2.3 (2.38–2.30)	40–3.5 (3.63–3.50)	40–3.2 (3.31–3.20)	40–3.2 (3.31–3.20)
Completeness (%)	92.3 (71.4)	93.8 (84.2)	81.0 (48.3)	98.9 (99.7)
R ^c (working set)	0.192 (0.244)	0.321 (0.363)	0.297 (0.370)	0.284 (0.327)
R _{free} ^d (test set)	0.223 (0.286)	0.373 (0.439)	0.346 (0.414)	0.366 (0.418)
B values				
Mean B value (overall, Å ²)	35.0	42.2	45.8	45.4
RMS deviations from ideal values				
Bond lengths (Å)	0.007	0.011	0.010	0.010
Bond angles (degrees)	1.56	1.69	1.58	1.44

^a $R_{\text{sym}} = \sum_j |I_j| / \langle I \rangle - I_j / \sum_j \langle I \rangle$, where I_j is the observed integrated intensity of the j th reflection and $\langle I \rangle$ is the average integrated intensity.

^b Values in parentheses refer to data in the highest resolution shell.

^c $R = \sum_{\text{hkl}} ||F_{\text{obs}}| - |F_{\text{calc}}|| / \sum_{\text{hkl}} |F_{\text{obs}}|$, where F_{obs} and F_{calc} are the observed and calculated structure factor amplitudes, respectively.

^d R_{free} is calculated with 5% of the reflection set aside randomly.

respectively. This structural similarity is reasonable since the sequence identity between the two enzymes is 54%. Some structural differences of peptide conformation were observed on the molecular surface which correlate with amino-acid sequence differences. The N-terminal half forms most of the myristoyl-CoA binding site, while the C-terminal half contributes largely to the peptide-substrate binding site, although the molecule is regarded as a single-domain structure. The bound conformation of myristoyl-CoA was almost the same as those of myristoyl-CoA and myristoyl-CoA analog in the complexes of *S. cerevisiae* Nmt. On the other hand, some conformational rearrangements were observed in the vicinity of the substrate binding site (see below).

In the ternary complex, the protein is observed as a dimer in which residues 60 to 81 of one molecule form an extended structure along the surface of the other molecule and vice versa, i.e., the N-terminal “tails” cross over (Figure 1). It is likely that for a monomer in solution, the N-terminal tail packs in a very similar way against the rest of the molecule. From the *S. cerevisiae* structure, the N-terminal 3₁₀-helix (A': residues 39 to 45 [27]) was

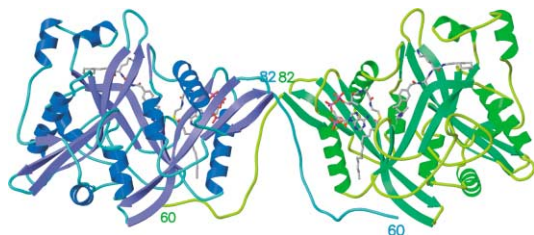


Figure 1. Ribbon Model of *C. albicans* Nmt in Complex with Myristoyl-CoA and SC-58272

Myristoyl-CoA and SC-58272 is shown as a stick model. Color codes of atoms are as follows: oxygen atoms, red; nitrogen atoms, blue; carbon atoms, gray.

presumed to be crucial for the recognition and binding of myristoyl-CoA [27]. However, in our structure, in which the N-terminal 59 residues were missing, the myristoyl-CoA binding has a similar conformation. Kinetic experiments showed that deletion of the amino-terminal 59 residues has no apparent effect on its activity in *in vitro* enzymatic assays. The dimer interactions observed in these crystals seem to be an artifact of crystallization and seem not to be related to the enzymatic activity.

Binding Mode of SC-58272, a Peptidic Inhibitor

A close-up view of the binding site of SC-58272 is presented in Figure 2A. The inhibitor lies in an extended conformation in a long groove formed by β strands and the loops of residues 238 to 249 of the C-terminal half and residues 106 to 115 of the N-terminal half. Moreover, the bound myristoyl-CoA itself forms a part of the binding site for SC-58272. A total of 84% (833 Å²) of the surface area of SC-58272 is buried in the long groove of the enzyme. This value is similar to those of the ternary complex of *S. cerevisiae* Nmt with a myristoyl-CoA analog and SC-58272. The bound conformation of the inhibitor is identical to that of SC-58272 in the complex of the *S. cerevisiae* Nmt [27]. The 2-methylimidazole group, which was designed to mimic the N terminus of a peptide substrate, is buried and interacts with the carboxyl group of the C-terminal residue (Leu451). The aliphatic chain between the imidazole ring and the benzene ring is bent and has contacts with myristoyl-CoA, thus guiding the imidazole ring to the C-terminal carboxylate. Several hydrophobic residues, Val108, Phe117, Tyr225, and Phe339, make van der Waals contacts with the benzene ring. The hydroxyl group of serine, which is completely buried, is hydrogen bonded to the side-chain imidazole group of His227 and to the main-chain amide group of Gly413. The amino group of lysine is surrounded by the side chains of negatively charged resi-

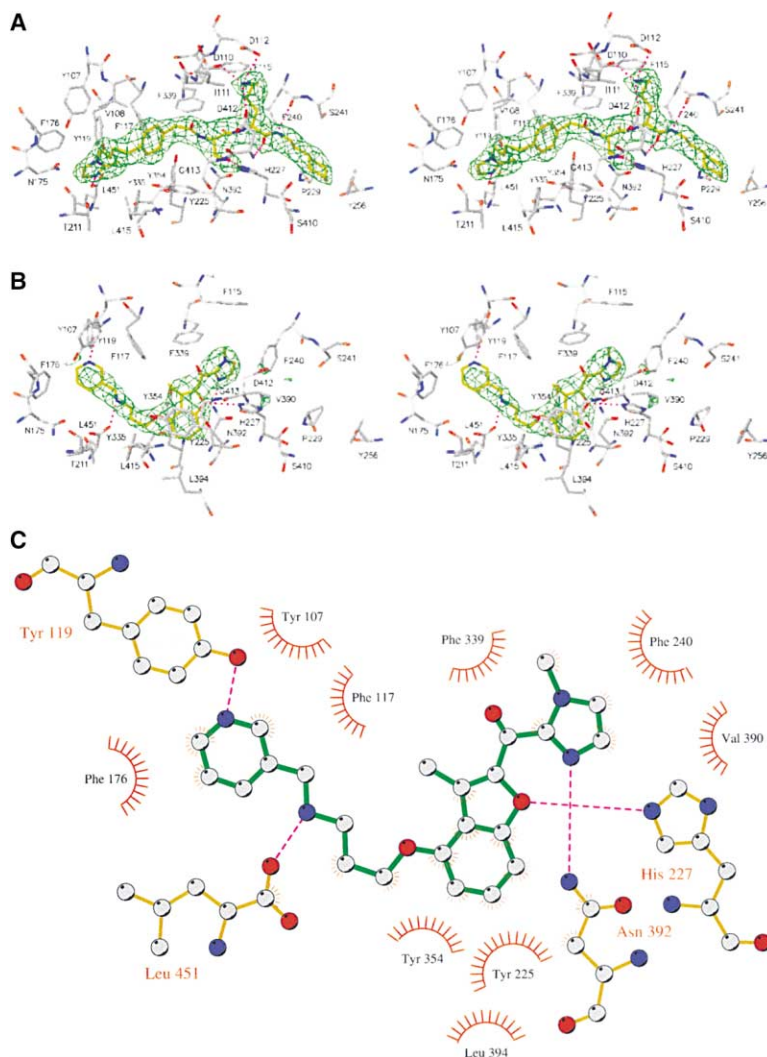


Figure 2. The Binding Mode of the Inhibitors
The inhibitors SC-58272 (A) and compound 5 (B) are outlined by the σ_A -weighted $F_o - F_c$ electron density map at the 3σ level with final model of the protein. Atoms are colored as in Figure 1, except that carbon atoms of the protein and the inhibitor are gray and yellow, respectively. Dashed magenta lines indicate hydrogen bond interactions. A schematic drawing of the interactions of compound 5 is shown in (C).

dues Asp110, Asp112, and Asp412. The aliphatic moiety of lysine is covered by the aromatic side chains of Phe115 and Phe240. The peptide moiety is also bound to the main-chain amide nitrogen and the side-chain carboxyl group of Asp412. The 2-cyclohexylethyl amide interacts with Pro229 and Tyr 256 and is positioned in an open-ended groove that would allow Nmt to accommodate a variety of substrate proteins.

Binding Mode of Nonpeptidic Inhibitors

The diffraction quality of crystals of *C. albicans* apo-enzyme used in soaking experiments was moderate. The electron density, however, was clear enough to elucidate the bound conformation of the inhibitors. A close-up view of the inhibitor binding site of the structure of *C. albicans* Nmt with compound 5 with an electron density map is shown in Figure 2B. The binding conformation of nonpeptidic inhibitors was examined with reference to the results of site-directed mutagenesis analysis (see below). As expected, the main-chain conformation was not changed by the soaking experiment (data not shown). Residues 108 to 113 of the Ab loop remain disordered on inhibitor binding. Crystal structures of

C. albicans Nmt with compounds 2 and 4 were also determined (Figure 3).

The nonpeptidic inhibitors are situated in the region of the substrate binding site, but with different interactions from those of SC-58272 (Figure 2C). The benzofuran moiety is located at the center of a deep pocket, surrounded by hydrophobic residues. The pocket of the inhibitor binding site is composed of aromatic residues Tyr107, Phe115, Phe117, Tyr119, Phe176, Tyr225, Phe240, Tyr256, Tyr335, Phe339, and Tyr354. The benzofuran ring is stacked parallel to Tyr225 and perpendicular to Tyr354 in the proximity of Phe117 and Phe339. These residues are presumed to be important not only for the architecture of the binding site but also for inhibitor binding. His227 is located in the proximity of the oxygen atom of the benzofuran ring. Since the inhibitor having a benzothiophene ring instead of a benzofuran ring showed about 1000-fold lower inhibitory activity, the hydrogen-bond interaction of the benzofuran ring with the imidazole ring of His227 and/or the geometry of the benzofuran ring might contribute to the inhibitor binding [22].

The secondary amine group of the substituent at posi-

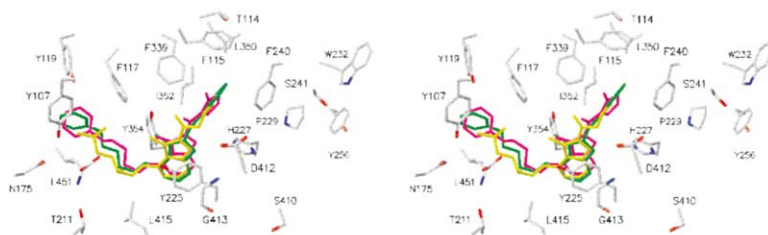


Figure 3. The Bound Conformation of Non-peptidic Inhibitors

The side-chain atoms of surrounding residues analyzed by site-directed mutagenesis, except for residues 108 to 113, are shown. The main-chain atoms of Gly413 are also shown. Compounds 2, 4, and 5 are shown in yellow, green, and magenta, respectively.

tion 4 of the benzofuran ring makes a hydrogen bond with the C-terminal carboxylate. This hydrogen bond formation accounts for our structure-activity relationships, which show that the secondary amine is essential for the inhibitory activity [21]. The conformation of the aliphatic chain between the secondary amine and the benzofuran ring is consistent with that elucidated by NMR spectroscopic analysis [31]. For the complex with compound 4, Tyr119 is in the proximity of the pyridine ring that is not contained in compound 2. It is known that the change of substituent from a tertiary butyl group to a 3-pyridylmethyl group improves the inhibitory activity [21]. The inhibition increase may be attributed to the additional hydrogen-bond interaction. The substituent at position 2 of the benzofuran ring is surrounded by the hydrophobic residues Phe115, Phe240, and Phe339. For the complex with compound 4, the 2,3-fluorophenyl group is situated adjacent to Phe240, with the fluorine atom positions on the phenyl ring not clearly defined. In the complex with compound 5, the methylimidazole ring makes a hydrogen-bond interaction with the side chain of Asn392 and is positioned in close proximity to Phe240. The substituent at position 2 is partially exposed to solvent, so that a bulky substituent seems to be acceptable for enzyme inhibition. These observations are consistent with chemical modification studies [21, 22]. The disordered Ab loop (residues 108 to 113) might also be in the proximity of the substituent at position 2, but no specific interaction was observed due to poor electron density.

Site-Directed Mutagenesis

A site-directed mutagenesis study was carried out in order to better characterize the bound conformation of the nonpeptidic inhibitors. A total of 29 mutants of residues located at the substrate binding site were produced. Only the mutant with Phe176 replaced by Ala (F176A) was insoluble; the other 28 mutants were expressed with almost the same level as the wild-type and were purified by the same procedure (Table 3 and Figure 3).

The inhibitory activity for mutants was estimated by the measurement of the K_i value for inhibitors. In this way, the relative contribution of residues in the substrate binding site to inhibitor binding may be estimated. The results for SC-58272 show that C-terminal carboxylate and the aromatic side chains of Phe115, Phe117, Tyr225, Phe240, and Tyr256 significantly affect binding (Table 3). These residues are presumed to be important not only for inhibitor binding but also for the architecture of the binding site, as the long groove is defined by these residues on binding of SC-58272. Asp112, His227, and Asp412 are also seen to function in inhibitor recognition.

The results of mutagenesis with SC-58272 agree with those of structural analysis.

Enzyme inhibition constants were measured for two nonpeptidic inhibitors, compounds 1 and 3 (Table 3). Mutants of three residues (F117A, Y354A, and L451 Δ) were significantly reduced in their inhibitor binding affinity for both inhibitors. These residues are localized in the substrate binding site. Y256A also showed reduced affinity for both inhibitors, although Tyr256 is found some distance away at the other end of the groove. This residue may significantly affect protein folding, as it was also observed that the enzymatic activity (V_{max}/K_m) was reduced by mutation of Tyr256 (data not shown). Replacement of the side chain of Leu451 had little effect on inhibition constants, while its deletion had a large effect. The crystal structures show that the side chain of Leu451 has no interaction with the nonpeptidic inhibitor. Different inhibition patterns for the two inhibitors may be correlated with their different substitution patterns. Alanine mutation of Tyr119 did not affect the K_i value of compound 1 but did affect that of compound 3. The crystal structures show that this tyrosine residue makes a hydrogen bond with the pyridine ring not contained in compound 1. Besides these residues, two more residues, Tyr225 and His227, seem to be involved in the inhibitor binding, as indicated by some changes of the K_i values. The crystal structures show that Tyr225 stacks with the benzofuran ring, being accompanied by structural rearrangement (see below), and that His227 is situated close to the benzofuran ring. In summary, the mutagenesis analysis identified several residues in the substrate binding site near to the enzyme C terminus which seem to be critical for the binding of nonpeptidic inhibitors.

Selectivity for Inhibitors

As shown in Table 1, a series of nonpeptidic inhibitors exhibited high inhibitory activity against *C. albicans* Nmt with low inhibitory activity against human Nmt. Such high selectivity between fungal and human Nmts is a prerequisite for a good antifungal drug. Identification of specific residues associated with selectivity will aid design of species-specific inhibitors of Nmts. The known crystal structures indicate that all Nmts have similar polypeptide folding. There are, however, a few specific amino-acid differences in the inhibitor binding site between *C. albicans* Nmt and other Nmts. Phe339 and Ile352 are replaced by serine and alanine, respectively, in human Nmt. Leu350 is replaced by valine in *A. fumigatus* Nmt. Leu451 is replaced by glutamine in human Nmt. High selectivity of the inhibitors might be caused by these differences of surrounding residues. Several mutants of *C. albicans* Nmt with a pseudo binding site from

Table 3. The Inhibitory Activity for Mutants of *C. albicans* Nmt

Compound	Enzyme Inhibition (K_i ; μ M)					
	SC-58272	1		3		
Wild type	0.25	0.60		0.03		
Mutants						
Y107A	2.0	(8.0)	1.7	(2.8)	0.07	(2.3)
V108A	0.15	(0.6)	0.69	(1.2)	0.07	(2.3)
D110A	3.2	(12.7)	0.39	(0.7)	0.03	(0.9)
I111A	0.35	(1.4)	2.6	(4.4)	0.46	(15.3)
D112A	10.6	(42.0)	0.14	(0.2)	0.03	(1.0)
T114A	0.08	(0.3)	0.45	(0.8)	0.04	(1.2)
F115A	>50	(>200)	0.28	(0.5)	0.02	(0.8)
F117A	>50	(>200)	>89	(>150)	>10	(>333)
Y119A	1.5	(5.9)	0.36	(0.6)	4.7	(158)
N175A	2.7	(10.7)	0.42	(0.7)	0.03	(1.0)
T211A	0.27	(1.1)	0.26	(0.4)	0.05	(1.7)
Y225A	>50	(>200)	2.2	(3.8)	0.46	(15.3)
H227A	7.4	(29.3)	1.9	(3.2)	3.2	(107)
P229A	0.30	(1.2)	0.54	(0.9)	0.05	(1.5)
W232A	0.84	(3.3)	0.45	(0.8)	0.10	(3.2)
F240A	>50	(>200)	0.24	(0.4)	0.09	(3.1)
S241A	0.77	(3.1)	1.1	(1.8)	0.24	(8.0)
Y256A	>50	(>200)	6.9	(11.5)	>10	(>333)
F339A	1.8	(7.3)	1.0	(1.7)	0.22	(7.3)
F339S					0.09	(3.1)
L350V	0.2	(0.7)			0.04	(1.3)
I352A	1.8	(7.3)	0.45	(0.8)	0.07	(2.2)
Y354A	2.2	(8.7)	>89	(>150)	>10	(>333)
D412A	21.8	(86.7)	0.05	(0.1)	0.03	(1.1)
G413A	0.18	(0.7)	0.86	(1.5)	0.11	(3.5)
L451A	0.25	(1.0)	0.54	(0.9)	0.15	(5.0)
L451Q	0.65	(2.6)			0.54	(18.0)
L451 Δ	>50	(>200)	>89	(>150)	>10	(>333)

The ratio of K_i values of mutant to that of wild-type are shown in parentheses.

different species were prepared in order to understand the difference of inhibitory activity for Nmts (F339S, L350V, I352A, and L451Q). No increase of the K_i value greater than 100-fold was observed for any single-residue mutation (Table 3). We conclude that the inhibitory specificity of the inhibitors is caused by more than one amino-acid difference. The selectivity is most likely a concerted effect of the residues that lie adjacent to the inhibitors. Therefore, structural information of human Nmt is necessary to rationalize the selectivity of these inhibitors.

Recognition of Inhibitors

The ternary complex of *C. albicans* Nmt with myristoyl-CoA and SC-58272 reveals the locations and interactions of myristoyl-CoA and the peptide substrate involved in the acyl transfer reaction. It was previously proposed that the ordered Bi-Bi reaction mechanism is attributed to the ordering and disordering of the Ab loop by myristoyl-CoA binding and CoA release, respectively [27, 28]. Our work supports this proposal. The apo-enzyme is known to have very low affinity for substrate protein or peptides, implying that the binding of myristoyl-CoA to the enzyme is required for the formation of a functional peptide binding site [32]. In the complex with nonpeptidic inhibitors, the Ab loop is disordered and makes no prominent interaction with the nonpeptidic inhibitor. The crystal structures also indicate that the nonpeptidic inhibitors can bind to the enzyme in

the absence of myristoyl-CoA, although kinetics studies indicate that the nonpeptidic inhibitor is competitive for peptide substrate binding [21]. It remains uncertain whether the nonpeptidic inhibitor is bound to the enzyme prior to the binding of myristoyl-CoA under physiological conditions. Myristoyl-CoA was not included in the soaking experiments purely because of solubility problems. The residues in which the inhibitory activity is diminished or abolished by site-directed mutagenesis are quite consistent with those which make interactions with the nonpeptidic inhibitors in the crystal structures. These considerations suggest that the bound conformation of the nonpeptidic inhibitor in the crystal is closely similar to that in solution. Even though nonpeptidic inhibitors have no interaction with the Ab loop, they showed quite strong inhibitory activity. We suggest that additional substituents designed to interact with the Ab loop might further improve enzyme inhibition.

The total solvent-accessible surface area of the substrate binding site of the apo-enzyme is larger than that of the complex with SC-58272, a substrate analog, which means that the substrate binding site of the apo-enzyme has greater exposure to solvent in comparison with the complex with peptide substrate. Comparison of the two structures reveals that the region of residues 114 to 120 (strand b) is shifted to cover the peptidic inhibitor (Figure 4A). Although the resolution level among structures is different, conformational changes are clear from this structural analysis. These conformational

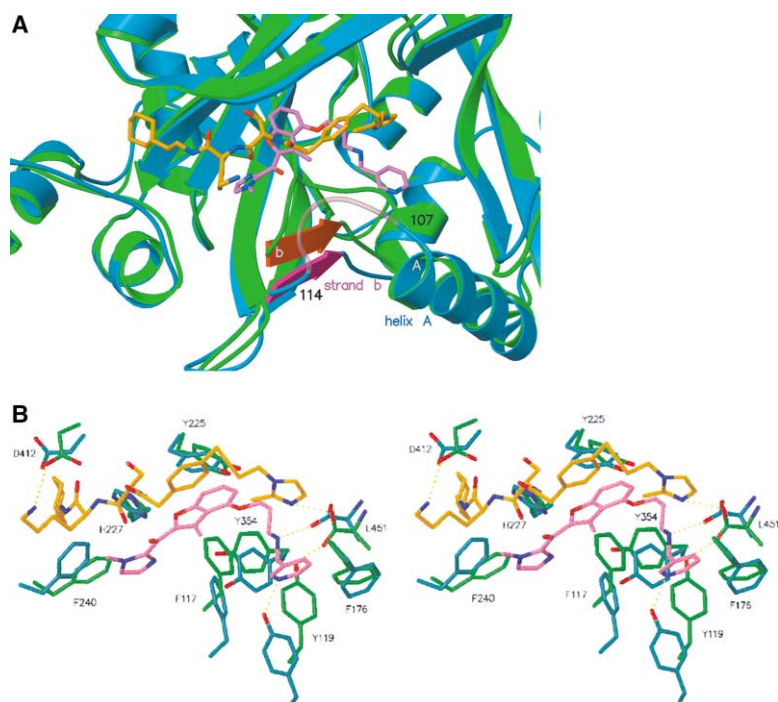


Figure 4. The Inhibitor Binding Site

(A) The secondary-structure differences. The structures of Nmt complexed with SC-58272 and with compound 5 are drawn in green and cyan, respectively. The inhibitors and β strand b [27] are highlighted in orange and magenta for each structure, respectively. The disordered Ab loop in the complex with compound 5 is transparent.

(B) The side-chain conformation differences. Hydrogen bonds are depicted with dashed yellow lines. Only side-chain atoms are drawn except those of the C-terminal residue (Leu451), in which only the main-chain atoms are drawn.

changes result in enlargement of the binding site and interaction with the secondary amine of the nonpeptidic inhibitor. The side-chain conformations in the vicinity of the inhibitor were compared between the complexes of the peptidic and nonpeptidic inhibitors (Figure 4B). A rearrangement of the side chain of Tyr225, which has no direct interaction with SC-58272, accompanies nonpeptidic inhibitor binding. Structural adjustments of aromatic residues Phe117, Tyr119, and Tyr354 were observed. These conformation changes indicate that the peptide substrate is trapped by the closure of the enzyme in the catalytic reaction and that the nonpeptidic inhibitor binds deep in the binding site and thus prevents peptide substrate binding. Further inhibitor design should be performed with the prospect of protein flexibility.

Significance

Myristoyl-CoA:protein *N*-myristoyltransferase (Nmt) attaches myristate to the proteins involved in a variety of signal transduction cascades and other critical cellular functions. The enzyme is essential for viability of *Candida albicans*, which is a major cause of systemic fungal infections in immunocompromised patients. Thus, Nmt is a potential target for the development of an antifungal drug. The crystal structures of *C. albicans* Nmt with peptidic and nonpeptidic inhibitors presented here contribute to understanding changes of the enzyme structure to enable substrate recognition and suggest ways in which the inhibitors might be improved. The enzyme has an opened conformation for substrate binding, and the nonpeptidic inhibitor prevents the adoption of a closed conformation. A comprehensive analysis of the substrate binding site demonstrates that the nonpeptidic inhibitor binds to

the substrate binding site surrounded by hydrophobic residues, making interactions different in detail from those made by the peptidic inhibitor. Site-directed mutagenesis studies have provided valuable information for the interpretation of the structure-activity relationships for a variety of inhibitors. The binding conformation of the inhibitor appears to be dominated by the interactions of its protonated amino group with the C-terminal carboxylate of the enzyme. However, it is currently impossible to state with certainty which residues contribute most to the species selectivity. Further structural analysis of other Nmts and chemical modification of inhibitors would help to solve this question.

Experimental Procedures

Expression and Purification

Nmt was produced in *E. coli* and purified as described previously [33] with an additional chromatography step. The gene coding for *C. albicans* Nmt was assembled into the T7 promoter expression plasmid (pT7-7, Stratagene). The *E. coli* strain BL21(DE3) (Stratagene) transformed by the Nmt expression plasmid was grown in modified Terrific Broth medium [1.2% tryptone, 1.2% yeast extract, 0.4% (v/v) glycerol, 40 mM phosphate buffer (pH 7.0)]. Protein expression was induced by IPTG (isopropyl- β -D-thiogalactopyranoside), and then the cells were harvested after incubation for a few hours at 37°C. All subsequent purification steps were carried out at 4°C. Wet cells were suspended into buffer A (30 mM MES [pH 6.5], 50 mM KCl, 2 mM EDTA, 2 mM PMSF [phenylmethylsulfonylfluoride]) and were sonicated followed by ultracentrifugation. The recombinant enzyme was purified from the lysate supernatants by cation-exchange chromatography on S-sepharose (Pharmacia) followed by chromatography on P11 phospho-cellulose column (Whatman) as described previously [12]. The purified enzyme was dialyzed against 30 mM MES (pH 6.5) for crystallization trials. The purity index of the final product was judged by SDS-PAGE. Alanine substitution mutants in the Nmt gene were programmed by site-directed mutagenesis using synthetic oligonucleotides. The presence of the de-

sired mutation was confirmed by DNA sequencing of the insert. The mutant enzymes were purified using the same protocol as described above.

Inhibitor Synthesis

SC-58272 was prepared by the method reported by Devadas et al. [20]. The analytical data were consistent with the structure. FAB-MS (*m*-nitrobenzyl alcohol), *m/z* 597 (*M*+*H*)⁺; ¹H-NMR, identical with the reported data. The purity of SC-58272 was confirmed by HPLC analysis using a TOSOH CCPS with Photol MCPD-3600 photodiode array detector (OHTSUKA ELECTRONICS) with an analytical column (MCI GEL ODS-1MU/4.6 × 150 mm). A gradient system of acetonitrile (pump A) and 0.015 M potassium phosphate buffer (pH 3.5) (pump B) was used. The gradient program was made up of linear segments (15/85 A/B to 98/2 A/B over 40 min), and the flow rate was 1.2 ml/min. SC-58272 was detected as a single peak at 10.2 min. Compounds 1–5 were prepared as previously described [21, 22].

Crystallization

In order to prepare a ternary Nmt:myristoyl-CoA:SC-58272 complex, the enzyme was concentrated to 60 mg/ml and was incubated with 5-fold excess molar of myristoyl-CoA and the inhibitor for a few hours at 4°C. Crystals were grown at 4°C in hanging drops over 10%–12% (w/v) polyethylene glycol 3350, 0.2 M ammonium acetate, and 50 mM HEPES (pH 7.5). Crystals generally appeared within 2–3 weeks with a maximum size of 0.6 × 0.6 × 0.2 mm. The result of the SDS-PAGE of the dissolved crystals showed that the molecular weight of the protein was about 45 kDa. The activity of the crystallized enzyme, however, remains the same as that of the starting material. The molecular weight of the crystallized enzyme was determined as 46 kDa by mass spectroscopy. The cleavage site of the enzyme, as determined by N-terminal amino-acid sequencing, was before residue Gln60. The crystals belong to the orthorhombic crystal system with space group *P*2₁2₁2₁ and unit-cell constants *a* = 58.7 Å, *b* = 95.3 Å, and *c* = 176.5 Å. There are two molecules in the asymmetric unit, with *V_m* [34] of 2.7 Å³/Da. In order to obtain complexes with the nonpeptidic inhibitors, soaking experiments were tried using these crystals. No conditions were found in which it was possible to displace SC-58272. Further, no cocrystals of the enzyme with the nonpeptidic inhibitors were obtained. In order to prepare complexes with the nonpeptidic inhibitors, crystals of the apo-enzyme were grown using a reservoir solution that contained 15%–18% (w/v) polyethylene glycol 3350, 0.2 M lithium sulfate, and 50 mM HEPES (pH 7.5). Inhibitors were soaked into the preformed crystals over a period of 3 hr using the reservoir solution containing 1% (v/v) DMSO. These crystals were of space group *P*2₁2₁2₁ with unit-cell dimensions *a* = 93.3 Å, *b* = 96.9 Å, and *c* = 269.3 Å. This unit cell gives a *V_m* of 3.4 Å³/Da for four molecules per asymmetric unit.

Data Collection and Processing

All diffraction data were collected at room temperature using crystals mounted in glass capillaries. The diffraction data of crystals of the complex with SC-58272 were collected on an imaging plate detector (MarResearch) mounted on a copper rotating-anode X-ray generator (ENRAF NONIUS FR591) equipped with double focusing optical mirrors (SUPPER). The data collection for heavy-atom derivatives was mainly done using a Hi-Star detector (Siemens) on a copper rotating-anode X-ray generator (ENRAF NONIUS FR571) with Ni filter. Data were processed using the program XDS [35]. The derivative data were scaled to the native data with SCALEIT from the CCP4 program suite [36]. The high-resolution data of the crystals of the ternary complex were collected up to 2.3 Å resolution on a Weissenberg camera [37] at beam line BL6B of Photon Factory (PF-KEK) and processed with the programs DENZO and SCALEPACK [38]. The data of crystals of the complex with nonpeptidic inhibitors were also collected at PF-KEK. The statistics are summarized in Table 2.

Structure Determination and Refinement

The structure of the complex with SC-58272 was solved by the method of multiple isomorphous replacement. Heavy atom derivatives were prepared by soaking crystals in solutions containing vari-

ous heavy atoms for set periods of time. For the first derivative, ethylmercury chloride, the positions of two sites were determined by direct inspection of difference Patterson maps using RSPS [36]. Sites for the second derivative, chloro(2,2′,2″-terpyridine) platinum (II), were determined by the use of difference Fourier maps, which were phased from the mercury derivative. Heavy atom parameters were refined with MLPHARE [39]. An initial MIR map at 15.3 Å resolution was calculated from the Hg and Pt derivative data, with mean figure-of-merit of 0.52. This electron density was modified by solvent flipping using SOLOMON [40] by solvent flattening with noncrystallographic symmetry averaging using DM [41] and phase extension to 2.7 Å. The resulting electron density map was of sufficient quality to interpret. An atomic model of the polypeptide chains was built using O [42] and Moloc [43]. Simulated annealing refinement followed by positional refinement and individual B factor refinement was performed at 2.3 Å resolution using the program CNX (Accelrys Inc.) with application of a bulk-solvent correction and with no amplitude cut-off. The free R factor was monitored as an indicator of model improvement throughout the refinement. The final model was examined using the program PROCHECK [44] and SFCHECK [45]. Solvent molecules were placed according to criteria of distance and a temperature factor.

The structure of the complex with nonpeptidic inhibitors was solved by molecular replacement using the structure with removed myristoyl-CoA and SC-58272 as a search model. A crossrotation function and a translation function using the monomer model (residues 82 to 451) were calculated by AMORE [46]. Four clear solutions were identified using data between 8.0–4.0 Å. The models were refined using positional refinement and grouped B factor refinement at 3.2 or 3.5 Å resolution by the programs CNX (Accelrys Inc.). The parameter and topology files for the nonpeptidic inhibitors were obtained using Moloc [43]. Noncrystallographic symmetry restraints were applied to residues 82 to 451. It was found that two molecules had significantly higher temperature factors than the others. After refinement of the polypeptide chains, examination of σ_A -weighted simulated-annealing omit maps [47] clearly indicated that the patches of strong residual electron density at the substrate binding site were interpretable as the inhibitor. The model of the inhibitor was built into the electron density using Moloc [43]. The final refinement statistics are listed in Table 2. The volume of the binding pocket for each structure was calculated using the program XSAE (C. Broger, personal communication).

The figures were generated using the programs MOLSCRIPT [48], RASTER3D [49], CONSCRIPT [50], and LIGPLOT [51].

Acknowledgments

We thank Drs. Suzuki and Igarashi and Prof. Sakabe at the Photon Factory for assistance with the beam line station (BL6B). S.S. and T.A.F. are members of Structure Biology Sakabe Project in Foundation for Advancement of International Science. Thanks are also due to Ms. F. Ford for proofreading the manuscript.

Received: June 24, 2002

Revised: September 9, 2002

Accepted: September 11, 2002

References

1. Rudnick, D.A., McWherter, C.A., Gokel, G.W., and Gordon, J.I. (1993). Myristoyl-CoA:protein N-myristoyltransferase. *Adv. Enzymol. Relat. Areas Mol. Biol.* 67, 375–430.
2. Boutin, J.A. (1997). Myristoylation. *Cell. Signal.* 9, 15–35.
3. Knoll, L.J., Johnson, D.R., Bryant, M.L., and Gordon, J.I. (1995). Functional significance of myristoyl moiety in N-myristoyl proteins. *Methods Enzymol.* 250, 405–435.
4. Olson, E.N., Towler, D.A., and Glaser, L. (1985). Specificity of fatty acid acylation of cellular proteins. *J. Biol. Chem.* 260, 3784–3790.
5. Wilcox, C., Hu, J.S., and Olson, E.N. (1987). Acylation of proteins with myristic acid occurs cotranslationally. *Science* 238, 1275–1278.
6. Johnson, D.R., Bhatnagar, R.S., Knoll, L.J., and Gordon, J.I.

- (1994). Genetic and biochemical studies of protein N-myristoylation. *Annu. Rev. Biochem.* 63, 869–914.
7. Towler, D.A., Gordon, J.I., Adams, S.P., and Glaser, L. (1988). The biology and enzymology of eukaryotic protein acylation. *Annu. Rev. Biochem.* 57, 69–99.
8. Resh, M.D. (1996). Regulation of cellular signalling by fatty acid acylation and prenylation of signal transduction proteins. *Cell. Signal.* 8, 403–412.
9. Zha, J., Weiler, S., Oh, K.J., Wei, M.C., and Korsmeyer, S.J. (2000). Posttranslational N-myristoylation of BID as a molecular switch for targeting mitochondria and apoptosis. *Science* 290, 1761–1765.
10. Farazi, T.A., Manchester, J.K., Waksman, G., and Gordon, J.I. (2001). Pre-steady-state kinetic studies of *Saccharomyces cerevisiae* myristoyl-CoA:protein N-myristoyltransferase mutants identify residues involved in catalysis. *Biochemistry* 40, 9177–9186.
11. Rudnick, D.A., McWherter, C.A., Rocque, W.J., Lennon, P.J., Getman, D.P., and Gordon, J.I. (1991). Kinetic and structural evidence for a sequential ordered Bi-Bi mechanism of catalysis by *Saccharomyces cerevisiae* myristoyl-CoA:protein N-myristoyltransferase. *J. Biol. Chem.* 266, 9732–9739.
12. Wiegand, R.C., Carr, C., Minnerly, J.C., Pauley, A.M., Carron, C.P., Langner, C.A., Duronio, R.J., and Gordon, J.I. (1992). The *Candida albicans* myristoyl-CoA:protein N-myristoyltransferase gene. Isolation and expression in *Saccharomyces cerevisiae* and *Escherichia coli*. *J. Biol. Chem.* 267, 8591–8598.
13. Lodge, J.K., Johnson, R.L., Weinberg, R.A., and Gordon, J.I. (1994). Comparison of myristoyl-CoA:protein N-myristoyltransferases from three pathogenic fungi: *Cryptococcus neoformans*, *Histoplasma capsulatum*, and *Candida albicans*. *J. Biol. Chem.* 269, 2996–3009.
14. Weinberg, R.A., McWherter, C.A., Freeman, S.K., Wood, D.C., Gordon, J.I., and Lee, S.C. (1995). Genetic studies reveal that myristoylCoA:protein N-myristoyltransferase is an essential enzyme in *Candida albicans*. *Mol. Microbiol.* 16, 241–250.
15. Lodge, J.K., Jackson-Machelski, E., Toffaletti, D.L., Perfect, J.R., and Gordon, J.I. (1994). Targeted gene replacement demonstrates that myristoyl-CoA:protein N-myristoyltransferase is essential for viability of *Cryptococcus neoformans*. *Proc. Natl. Acad. Sci. USA* 91, 12008–12012.
16. Duronio, R.J., Reed, S.I., and Gordon, J.I. (1992). Mutations of human myristoyl-CoA:protein N-myristoyltransferase cause temperature-sensitive myristic acid auxotrophy in *Saccharomyces cerevisiae*. *Proc. Natl. Acad. Sci. USA* 89, 4129–4133.
17. Sikorski, J.A., Devadas, B., Zupiec, M.E., Freeman, S.K., Brown, D.L., Lu, H.F., Nagarajan, S., Mehta, P.P., Wade, A.C., Kishore, N.S., et al. (1997). Selective peptidic and peptidomimetic inhibitors of *Candida albicans* myristoylCoA:protein N-myristoyltransferase: a new approach to antifungal therapy. *Biopolymers* 43, 43–71.
18. Devadas, B., Freeman, S.K., McWherter, C.A., Kishore, N.S., Lodge, J.K., Jackson-Machelski, E., Gordon, J.I., and Sikorski, J.A. (1998). Novel biologically active nonpeptidic inhibitors of myristoylCoA:protein N-myristoyltransferase. *J. Med. Chem.* 41, 996–1000.
19. Lodge, J.K., Jackson-Machelski, E., Higgins, M., McWherter, C.A., Sikorski, J.A., Devadas, B., and Gordon, J.I. (1998). Genetic and biochemical studies establish that the fungicidal effect of a fully depeptidized inhibitor of *Cryptococcus neoformans* myristoyl-CoA:protein N-myristoyltransferase (Nmt) is Nmt-dependent. *J. Biol. Chem.* 273, 12482–12491.
20. Devadas, B., Freeman, S.K., Zupiec, M.E., Lu, H.F., Nagarajan, S.R., Kishore, N.S., Lodge, J.K., Kuneman, D.W., McWherter, C.A., Vinjamoori, D.V., et al. (1997). Design and synthesis of novel imidazole-substituted dipeptide amides as potent and selective inhibitors of *Candida albicans* myristoylCoA:protein N-myristoyltransferase and identification of related tripeptide inhibitors with mechanism-based antifungal activity. *J. Med. Chem.* 40, 2609–2625.
21. Masubuchi, M., Kawasaki, K., Ebiike, H., Ikeda, Y., Tsujii, S., Sogabe, S., Fujii, T., Sakata, K., Shiratori, Y., Aoki, Y., et al. (2001). Design and synthesis of novel benzofurans as a new class of antifungal agents targeting fungal N-myristoyltransferase. Part 1. *Bioorg. Med. Chem. Lett.* 11, 1833–1837.
22. Ebiike, H., Masubuchi, M., Liu, P., Kawasaki, K., Morikami, K., Sogabe, S., Hayase, M., Fujii, T., Sakata, K., Shindoh, H., et al. (2002). Design and synthesis of novel benzofurans as a new class of antifungal agents targeting fungal N-myristoyltransferase. Part 2. *Bioorg. Med. Chem. Lett.* 12, 607–610.
23. Armour, D.R., Bell, A.S., Kemp, M.I., Edwards, M.P., and Wood, A. (2001). Discovery of a novel series of nonpeptidic fungal N-myristoyltransferase inhibitors. *Abstr. Pap. Am. Chem. Soc., MEDI-349*.
24. Bell, A.S., Armour, D.R., Edwards, M.P., Kemp, M.I., and Wood, A. (2001). Discovery of fungicidal N-myristoyltransferase inhibitors. *Abstr. Pap. Am. Chem. Soc., MEDI-350*.
25. Ganesh, K.R., and Madhavao, K.V. (2001). Computer-aided design and synthesis of *Candida albicans* N-myristoyltransferase inhibitors as antifungal agents. *Indian Drugs* 38, 406–413.
26. Weston, S.A., Camble, R., Colls, J., Rosenbrock, G., Taylor, I., Egerton, M., Tucker, A.D., Tunnicliffe, A., Mistry, A., Mancina, F., et al. (1998). Crystal structure of the anti-fungal target N-myristoyltransferase. *Nat. Struct. Biol.* 5, 213–221.
27. Bhatnagar, R.S., Futterer, K., Farazi, T.A., Korolev, S., Murray, C.L., Jackson-Machelski, E., Gokel, G.W., Gordon, J.I., and Waksman, G. (1998). Structure of N-myristoyltransferase with bound myristoyl-CoA and peptide substrate analogs. *Nat. Struct. Biol.* 5, 1091–1097.
28. Farazi, T.A., Waksman, G., and Gordon, J.I. (2001). Structures of *Saccharomyces cerevisiae* N-myristoyltransferase with bound myristoyl-CoA and peptide provide insights about substrate recognition and catalysis. *Biochemistry* 40, 6335–6343.
29. Bhatnagar, R.S., Futterer, K., Waksman, G., and Gordon, J.I. (1999). The structure of myristoyl-CoA:protein N-myristoyltransferase. *Biochim. Biophys. Acta* 1441, 162–172.
30. Devadas, B., Zupiec, M.E., Freeman, S.K., Brown, D.L., Nagarajan, S., Sikorski, J.A., McWherter, C.A., Getman, D.P., and Gordon, J.I. (1995). Design and syntheses of potent and selective dipeptide inhibitors of *Candida albicans* myristoyl-CoA:protein N-myristoyltransferase. *J. Med. Chem.* 38, 1837–1840.
31. Miura, T., Klaus, W., Ross, A., Sakata, K., Masubuchi, M., and Senn, H. (2001). Protein-bound conformation of a specific inhibitor against *Candida albicans* myristoyl-CoA:protein N-myristoyltransferase in the ternary complex with CaNmt and myristoyl-CoA by transferred NOE measurements. *Eur. J. Biochem.* 268, 4833–4841.
32. Bhatnagar, R.S., Schall, O.F., Jackson-Machelski, E., Sikorski, J.A., Devadas, B., Gokel, G.W., and Gordon, J.I. (1997). Titration calorimetric analysis of Acyl-CoA recognition by myristoyl-CoA:protein N-myristoyltransferase. *Biochemistry* 36, 6700–6708.
33. Duronio, R.J., Towler, D.A., Heuckeroth, R.O., and Gordon, J.I. (1989). Disruption of the yeast N-myristoyltransferase gene causes recessive lethality. *Science* 243, 796–800.
34. Matthews, B.W. (1968). Solvent content of protein crystals. *J. Mol. Biol.* 33, 491–497.
35. Kabsch, W. (1993). Automatic processing of rotation diffraction data from crystals of initially unknown symmetry and cell constants. *J. Appl. Crystallogr.* 26, 795–800.
36. Bailey, S. (1994). The CCP4 suite: programs for protein crystallography. *Acta Crystallogr. D* 50, 760–763.
37. Sakabe, K., Sasaki, K., Watanabe, N., Suzuki, M., Wang, Z.G., Miyahara, J., and Sakabe, N. (1997). Large-format imaging plate and Weissenberg camera for accurate protein crystallographic data collection using synchrotron radiation. *J. Synchrotron Radiat.* 4, 136–146.
38. Otwinowski, Z. (1993). Oscillation data reduction program, pp. 56–62. In *Proceedings of the CCP4 Study Weekend (Data Collection and Processing)*, L. Sawyers, N. Isaacs, and S. Bailey, eds. Daresbury, UK, SERC.
39. Otwinowski, Z. (1991). Maximum likelihood refinement of heavy atom parameters, pp. 80–85. In *Proceedings of the CCP4 Study Weekend (Isomorphous Replacement and Anomalous Scattering)*, W. Wokt, P.R. Evans, and A.G. Leslie, eds. Daresbury, UK, SERC.
40. Abrahams, J.P., and Leslie, A.G.W. (1996). Methods used in

- the structure determination of bovine mitochondrial F1 ATPase. *Acta Crystallogr. D* 52, 30–42.
41. Cowtan, K. (1994). 'dm': An automated procedure for phase improvement by density modification. In Joint CCP4 and ESF-EACBM Newsletter on Protein Crystallography, pp. 34–38.
 42. Jones, T.A., Zou, J.Y., Cowan, S.W., and Kjeldgaard, M. (1991). Improved methods for binding protein models in electron density maps and the location of errors in these models. *Acta Crystallogr. A* 47, 110–119.
 43. Gerber, P.R. (1992). Peptide mechanics: a force field for peptides and proteins working with entire residues as smallest units. *Biopolymers* 32, 1003–1017.
 44. Laskowski, R.A., MacArthur, M.W., Moss, D.S., and Thornton, J.M. (1993). PROCHECK: a program to check the stereochemical quality of protein structures. *J. Appl. Crystallogr.* 26, 283–291.
 45. Vaguine, A.A., Richelle, J., and Wodak, S.J. (1999). SFCHECK: a unified set of procedures for evaluating the quality of macromolecular structure-factor data and their agreement with the atomic model. *Acta Crystallogr. D* 55, 191–205.
 46. Navaza, J. (1994). AMoRe: an automated package for molecular replacement. *Acta Crystallogr. A* 50, 157–163.
 47. Read, R.J. (1986). Improved Fourier coefficients for maps using phases from partial structures with errors. *Acta Crystallogr. A* 42, 140–149.
 48. Kraulis, P.J. (1991). MOLSCRIPT: a program to produce both detailed and schematic plots of protein structures. *J. Appl. Crystallogr.* 24, 945–949.
 49. Merritt, E.A., and Murphy, M.E.P. (1994). Raster3D version 2.0. A program for photorealistic molecular graphics. *Acta Crystallogr. D* 50, 869–873.
 50. Lawrence, M.C., and Bourke, P. (2000). CONSCRIPT. A program for generating electron density isosurfaces for presentation in protein crystallography. *J. Appl. Crystallogr.* 33, 990–991.
 51. Wallace, A.C., Laskowski, R.A., and Thornton, J.M. (1995). LIGPLOT: a program to generate schematic diagrams of protein-ligand interactions. *Protein Eng.* 8, 127–134.

Accession Numbers

The coordinates of the complexes with SC-58272 and compound 5 have been deposited in the Protein Data Bank under ID codes 1IYK and 1IYL, respectively.